Measurements of ambient seabed seismic levels below 1.0 Hz on the shallow eastern U.S. continental shelf

Mark V. Trevorrow, Tokuo Yamamoto, Altan Turgut, and Dean Goodman
Division of Applied Marine Physics, Rosenstiel School of Marine and Atmospheric Science, University of Miami, 4600 Rickenbacker Causeway, Miami, Florida 33149

(Received 25 May 1989; accepted for publication 19 August 1989)

Measurements of ambient seismic noise levels in the range 0.03–1.0 Hz were made using ocean-bottom seismometers (OBS) at four shallow-water (<100 m) locations on the New Jersey Shelf and George's Bank. Surface gravity-wave-induced seabed motion (single-frequency microseism) was found to be dominant in the frequency range 0.03–0.3 Hz, with the high-frequency cutoff strongly dependent on water depth. The peak seismic level in the water wave band was measured at 2.0×10^{-8} $(\mathrm{m/s^2})^2$/Hz in 12 m of water. This level was observed to decrease rapidly with greater water depth. Seismic interface waves (microseisms) of power level approximately 5×10^{-10} $(\mathrm{m/s^2})^2$/Hz were observed in the range 0.25–1.0 Hz. This microseism power level was found to be roughly constant in water depths from 12 to 70 m. A quiet "notch" between the two wave bands, in the range 0.15–0.3 Hz, was observed. The background seismic level in this notch was determined to be less than 5×10^{-12} $(\mathrm{m/s^2})^2$/Hz. Extrapolations of the observed pressures and seabed motions into deeper water conditions are made.

PACS numbers: 43.30.Nb, 43.40.Ph

INTRODUCTION

There has been considerable interest over the past 30 years in the cause and levels of ambient seismic noise in the ocean sediments. This work has been motivated by interest in the coupling between both surface gravity and acoustic waves and the seabed sediments, and a need to know the background noise levels as a precursor to increasing the global coverage of seismic monitoring stations. The majority of ocean-bottom seismometer (OBS) deployments have focused on deep-ocean (>2000 m) environments and frequencies in the range 1–20 Hz.[1–11] The seismic motions of the shallow-water (<100 m) seabed sediments at frequencies below 1.0 Hz are essentially unknown.

Due to the difficulty in working in the deep-ocean environment, the typical OBS design has been robust, heavy, and capable of operating self-sufficiently (internal power and recording) for periods of months. The combination of large and heavy OBS packages resting on very soft, water-saturated sediments has produced significant problems with OBS-to-sediment coupling. In essence, an OBS/sediment system has been shown to behave like a damped harmonic oscillator, with resonant frequencies of the order of 10 Hz (Sutton *et al.*,[12] Sutton and Duennebier[13]). Furthermore, since a typical OBS package has a large hydrodynamic cross section (large-pressure housing, floatation spheres, antennas, and recovery aids), it is very effectively coupled to water currents and highly susceptible to "added-mass" effects (Trevorrow *et al.*[14]). These problems exist in both deep- and shallow-ocean environments, and have to date been major obstacles to the accurate measurement of seabed seismic activity.

The shallow continental margins of the world's oceans are areas of abundant ambient seismic activity at frequencies below 1.0 Hz. The proximity of the ocean surface with the bottom accentuates wave phenomena that are not normally of consequence in the deep ocean. The typical sediment displacement amplitude in shallow waters is of the order of 100 μ (Trevorrow *et al.*[15]). This can be compared to typical Pacific deep-ocean amplitudes of 100 nm (Hedlin and Orcutt[5]) and an amplitude of $\approx 1\ \mu$ measured in the deep Atlantic near Bermuda (Latham and Sutton[6]). These measured deep-ocean amplitudes are obviously site and weather dependent.

The most significant difference beween deep- and shallow-water conditions is the prominence of so-called "single-frequency" microseisms. This type of sediment motion is a direct response to surface gravity- (SG) wave-induced pressure variations on the seabed. SG waves begin to cause measurable seabed displacements when they reach water depths roughly equal to their wavelength. This SG-wave-induced seabed motion is predominant in the frequency range 0.05–0.3 Hz (3–20 s), depending on the water depth.

This single-frequency seabed motion is several orders of magnitude larger than, and thus obscures, the usual double-frequency microseism energy measured in the deep ocean[1–11] and at coastal (onshore) sites[16–18] at frequencies in the range 0.1–0.5 Hz. These motions are called "double-frequency" (DF) because their peak power densities lie at twice the frequency of concurrent SG waves. Nonlinear SG-wave interactions, as proposed by Longuet-Higgins,[19] Hasselmann,[20] and Kadota and Labianca,[21] are the probable driving mechanisms for this type of sediment motion. DF pressure variations are theoretically attenuated very little with increasing water depth and have been measured in the deep ocean by Latham *et al.*,[22] and Webb and Cox.[11] These

DF microseisms are thought to be sediment/water interface waves of the Scholte type (Latham and Sutton,[6] Latham and Nowroozi,[7] and Goodman *et al.*[23]). As we shall show, in shallow waters these DF microseisms are observed at higher frequencies (> 0.2 Hz) than in the deep ocean.

The accurate measurement of ambient seismic noise levels on the shallow continental shelf is obviously important to any active (reflection, refraction surveys) or passive seismology. For example, Stoll *et al.*[24] have recently performed active shear-wave refraction surveys in shallow waters to remotely sense sediment properties. Furthermore, it has become apparent recently that there is a strong coupling between very-low-frequency (VLF) acoustic noise fields and sediment motions (Urick,[25] Brocher and Iwatake,[4] and Kibblewhite and Ewans[18]). As an example, Schmidt and Kuperman[26] have demonstrated that seismic interface waves are important propagation paths for ambient acoustic noise below the water-borne cutoff frequency in shallow water. Recently, Kibblewhite and Wu[27,28] have developed theoretical expressions linking surface gravity waves, infrasonic acoustic noise, and seabed microseisms. Thus accurate measurement of the seismic noise field is necessary for the prediction of VLF acoustic noise levels.

Our interest in the nature and levels of this shallow-water seismic activity comes from experimental development of seabed-sediment remote-sensing techniques. Through measurement of the SG-wave-induced pressure and seabed displacement, it is possible to extract the seabed-sediment shear-modulus profile (Yamamoto and Torii,[29] Trevorrow *et al.*[15]). We call this sediment remote-sensing method, and the OBS package used in the experiments, the bottom shear-modulus profiler (BSMP). Through the use of an empirical relation, the seabed porosity (and hence bulk density and shear-wave velocity) profile can be calculated from the shear modulus (Yamamoto *et al.*[30]). Further extensions to the BSMP method are under development.

The seabed seismic and pressure levels reported in this paper come directly from several years of experiments to test and improve the BSMP method (reported in Trevorrow *et al.*[31,32]). The purpose of this paper is to summarize the results of these experiments. As a necessary prelude to the presentation of results, we will describe the instrumentation and experimental procedures developed for the BSMP method. To negate the usual OBS/sediment coupling problems, we have developed a method for shallow burial of the seismometer packages in the seabed sediments. All of the results shown in this paper come from buried BSMP units. For brevity, only the vertical components of seabed acceleration will be shown, as the behavior of the horizontal components is similar. Finally, we will make some simple extrapolations of the measured pressures and seabed motions to deeper water conditions, showing that our results are consistent with previously reported deep-ocean measurements.

I. INSTRUMENTATION

Our experiments were aimed at measuring the total seabed acceleration and sea-bottom wave-induced pressures in the VLF range 0.01–1.0 Hz. For this purpose, we developed two similar shallow-water OBS systems, one analog and one digital, known as bottom shear-modulus profilers (BSMPs).

The BSMP unit has undergone several sets of experiments and redesigns, leading to the high-resolution (HR-) BSMP. The technical information on the HR-BSMP can be found in Turgut *et al.*[33] Basically, the HR-BSMP consists of two separate housings connected by a 2-m umbilical cable. The seismometer housing is a hollow aluminum alloy cylinder (diameter = 30.5 cm, height = 25.5 cm). It contains three orthogonally mounted seismometers (Teledyne-Geotech model S-750) and two pendulum tiltmeters (Sperry model 02383-01). The seismometers have a peak resolution of 10^{-8} m/s^2 and a flat response down to 0.01 Hz ($-$ 3-dB point). As will be explained later, the seismometer housing is designed to be buried in the surficial seabed sediments to obtain maximal coupling. The umbilical cable carries power to the instruments, the output signals, and a calibration signal used to excite internal coils in the seismometers. This internal seismometer calibration capability is most useful in checking for proper seismometer function after deployment to the seabed.

The second housing is a flat aluminum cylinder (diameter = 30.5 cm, height = 9.0 cm) designed to remain on the seabed surface and support the differential pressure sensor. It also serves as a junction between the 12-conductor umbilical and a 16-conductor main electro-mechanical cable that connects to the accompanying ship. The pressure sensor itself (InterOcean model WS200) is designed to measure VLF water pressure fluctuations at depths up to 200 m. The pressure sensor has a resolution threshold of 10 Pa and a flat frequency response down to 0.002 Hz.

The three seismometer accelerations and the pressure signal are bandpass filtered between 0.004 and 0.5 Hz using second-order filters. The frequency responses of the instruments and filters are combined, and used to correct the measured power and cross spectra in the later data-processing stages. The four signals from a HR-BSMP unit are recorded in an FM analog mode using a TEAC SR-51 14-channel data recorder. The frequency response of the seismometer system (S-750 instrument, amplifier, and filter) is shown in Fig. 1. The pressure response, due mostly to the same bandpass filters and amplifiers, is similar.

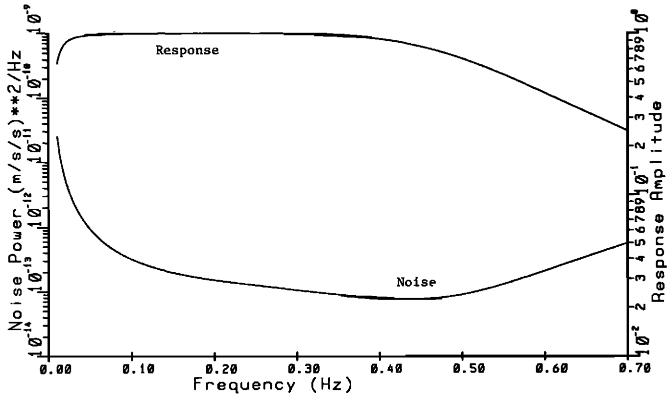

FIG. 1. Frequency response and noise power levels for S-750 seismometers, amplifiers, filters, and recording system.

For the design of the BSMP, we chose to locate all of the power supplies, bandpass filters, amplifiers, and recording equipment on board the ship. The BSMP units are connected to the ship via 16-conductor electromechanical cables. This remote monitoring scheme has several advantages. The seismometer housing itself need be only big enough to contain three seismometers, two tiltmeters, and a compass. Remote monitoring allows the acceleration and pressure signals to be examined before and during recording. Amplifier gains can be adjusted and BSMP/sediment coupling quality can be examined before taking any data. In some instances, a poorly deployed BSMP (badly tilted, upside down, etc.) can be detected and redeployed correctly. Also, the recorded data is never lost at sea should the OBS recovery operation be unsuccessful. Tethering an OBS to the ship is obviously difficult in ocean environments, but has been previously attempted with some success (Latham and Nowroozi,[7] Adair *et al.*[1]).

A variant of the BSMP design uses digital radiotelemetry from a surface buoy instead of tethering directly to the ship. The technical information on this system is given by Abbott *et al.*[34] The seismometer housings for this system are identical and interchangeable with those of the analog system. The major difference is a larger electronics housing, containing filters, amplifiers, and digitizing electronics. The digitization rate is set at 4 Hz. Attached to the electronics housings is a differential pressure sensor (PME model 109, function described by Cox *et al.*[35]). The PME differential pressure sensor has a flat response down to 0.00723 Hz (− 3-dB point). All instruments are bandpass filtered using second-order filters (0.004–0.5 Hz, same as analog system). Thus the frequency response of the digital system is nearly identical to that of the analog system. The four digital signals (three seismometers and pressure) are multiplexed, then taken via coaxial cables to a surface buoy, where they were then relayed via FM radiotelemetry to the attending ship. Each surface buoy can support two BSMP instruments. The digital radiotelemetry BSMP units were used only in the 1988 experiments. Because they are not tethered directly to the ship, the digital BSMP units are more easily deployed in rough weather.

An important quantity necessary in the interpretation of the experimental results is the internal, systemic noise level. Obviously, seismic and pressure signals comparable to these internal noise levels cannot be accurately measured, and this turns out to be a major limitation of the system at frequencies lower than 0.03 Hz. The detailed calculations of the noise power levels in the entire BSMP system are too lengthy to be produced here. In short, the broadband noise power spectrum from each source is calculated, corrected for the appropriate filter responses and amplifier gains, then added together.

The sources of internal noise included in the calculations are the following: (1) Shot, flicker, and thermal noise in the seismometers, pressure sensor, and amplifier/filter electronics. Each resistor in the circuitry acts as a white thermal noise generator. Shot and flicker noise are induced in the transistor amplifiers by small leakage currents, and both have a $1/f$ frequency dependence. (2) Tape hiss, flutter, and amplifier noise in the FM data recorder. (3) Quantizing noise in the digitizer. These calculations do not include noise voltages induced in the piezoelectric crystal of the S-750 seismometer, which are difficult to quantify. This may be a significant noise source at frequencies lower than 0.03 Hz. The low-frequency noise is dominated by the electronic noise voltages, while near 1.0 Hz, quantizing noise and tape effects dominate. Figure 1 shows the noise power spectrum predicted for the S-750 seismometer and its electronics. The noise characteristics of the differential pressure system (either InterOcean WS-200 or PME-109), due mostly to the same amplifiers, filters, and tape recorders, are similar in form. These noise levels should be considered as absolute "basement" levels. Significantly more noncoherent noise may be produced in real ocean environments by "coupling noise" (cable tugs on BSMP, BSMP settling into sediments, earthquakes, and other transients), especially at lower frequencies.

In addition to making laboratory predictions of the internal noise levels, we performed a unique *in situ* test of the actual systemic noise. In July 1988 at the George's Bank site, a digital radiotelemetry BSMP was deployed with three vertically oriented seismometers in the same housing. This situation provided three independent measurements of the same vertical seabed acceleration, with electronic noise added by each independent (yet identical) seismometer, amplifier, and filter combination. In this way, the strength of the internal noise relative to a real ocean signal level across the entire VLF frequency band can be assessed.

The cross-spectral coherence $\gamma^2(f)$ (calculation details given in Sec. II A) between two of these vertical acceleration signals, as shown in Fig. 2, quantifies the noise contamination. For uncontaminated signals, the coherence will approach 1.0. The noise power level in the measured signal is $(1-\gamma^2)$ times the measured acceleration power spectrum. Thus a signal/noise ratio of 1.0 corresponds to a coherence value of 0.5. As can be seen from the figure, the uncontaminated frequency bands are 0.03–0.15 and 0.3–0.7 Hz (actually extends up to 0.95 Hz). These bands are regions of high signal level, as shown in Fig. 3, which show the time-averaged power spectrum from one of the three vertical seismometers (all three are identical). Notice that the coherence

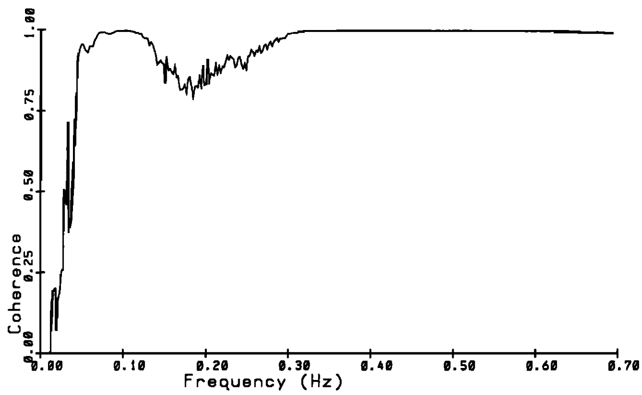

FIG. 2. Coherence between two vertical seismometers in the same housing at the George's Bank site, 17 July 1988. Time averaged over 56 segments (8 h).

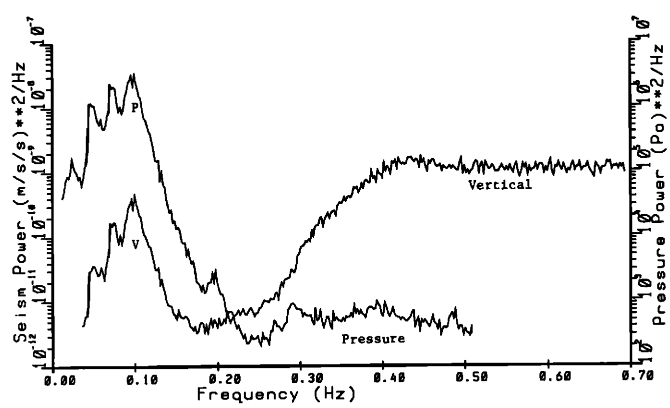

FIG. 3. Time-averaged vertical seismometer and seabed pressure power spectra from George's Bank site. Water depth = 51 m. Averaged over 56 time segments.

falls below 1.0 in frequency bands where the seismic signal falls below 5.0×10^{-12} $(m/s^2)^2/Hz$. This may be taken as a basement noise power level in the entire system. It is thought possible that piezoelectric crystal noise in the S-750 seismometer is responsible for this noise level. All seismic spectra presented in this paper will have components below 0.03 Hz (33 s) removed because of this noise contamination. Also, all pressure spectral components above 0.5 Hz (2 s) are removed because of low signal levels being dominated by internal noise.

II. EXPERIMENTS

A. Locations and deployment procedures

The HR-BSMP system has been tested in sea experiments over the past 2 years (1987 and 1988) at various water depths and on different seabed sediments. A summary of the experimental locations is given in Table I. Over 500 h of three-component seismometer and pressure data have been collected during these experiments. These locations were selected for their proximity to previously conducted sediment-coring experiments conducted by the U.S.G.S. and others. At all sites, the seabeds were known to be composed of many hundreds of meters of sand and silty sand sediments. BSMP units were deployed in arrays on the seabed (up to nine units). The use of arrays enabled the measurement of the directional spectra and propagational characteristics of both long-period surface gravity waves and microseisms.

The accurate measurement of the very-low-frequency seabed motions found in shallow continental margin sediments is not a trivial problem. The shallow waters are areas of large water-current activity. Strong and slowly varying currents are induced by tides. This was especially a problem at the George's Bank site. Also, surface gravity waves induce oscillating horizontal currents near the seabed. Any OBS design must negate the effects of these fluctuating water currents, while at the same time returning highly accurate measurements of the seabed motions.

In addition, Sutton *et al.*[12] specified that for good OBS-to-sediment coupling, a design should have a density similar to that of the sediment, a large sediment contact area, and a small and smooth cross section in the water. The OBS-sediment resonant coupling theory presented by Sutton *et al.*[12,13] suggested that a neutral density in sediment, buried OBS would show perfect coupling at nearly any frequency (their theory is valid for shear wavelengths greater than four times the OBS radius. For OBS radius = 0.15 m and sediment shear speed = 50 m/s, this implies frequencies less than 83 Hz). We chose to follow this prediction by designing a hydraulic burial apparatus that implants the BSMP seismometer housing up to 50 cm into the sediments. The density of the BSMP seismometer housing was matched to the bulk density of the sandy marine sediments (approximately 2000 kg/m^3) commonly found on the eastern U.S. continental shelf. Burial of the seismometer housing also negates the effects of near-bottom water currents. The authors have found that burial of the seismometer housing in the sediments is the only successful method of obtaining good coupling characteristics in shallow water (Trevorrow *et al.*[14]). All results shown in this paper come from buried seismometer housings.

Burial of the seismometer housing is achieved through the use of a hydraulic jet burial system, developed by the authors.[14,33] Basically, the burial system consists of a vertical, three-pronged burial bracket that cradles the seismometer housing. This burial bracket is held upright by a 1.2-m-diam steel support dome, which allows vertical motion of the bracket only. The pressure sensor housing is suspended outside the burial dome and remains on the seabed during the data collection. An electromagnet release mechanism, controlled from the ship, uncouples the two housings from the burial dome when the system reaches the seabed. Seawater is pumped (700 kPa, 0.01 m^3/s) through the prongs of the burial bracket using a 3.75-kW submersible electric pump (Grundfos model SP16-5). Water jets at the prong tips liquify the sediments and excavate the sediments from underneath the seismometer housing. The burial bracket and seismometer housing sink under their own

TABLE I. Locations of BSMP experiments 1987 and 1988.

Site	Latitude (north)	Longitude (west)	Depth (m)	Date	Number of instruments deployed
AGS	39° 28′	74° 15′	11-13	29–30 Aug. 1987	7
				7–10 July 1988	9
AMCOR 6009	38° 51′	73° 36′	58	2–3 Sept. 1987	6
AMCOR 6010	39° 03′	73° 07′	68-70	3 Sept. 1987	2
				13–14 July 1988	5
George's Bank	40° 56′	68° 18′	51-53	15–18 July 1988	4

weight into the sediments, with the excess sediments filling in on top of the seismometer housing. After burial, the dome and bracket are hauled back up to the ship so as not to interfere with seabed motions and pressures. The entire burial operation takes less than 3 min and has been successfully performed in water depths up to 70 m.

B. Data processing

The three components of seabed acceleration and the bottom hydrodynamic pressure need to undergo extensive spectral averaging before they can be intelligently used. This is done to handle the random nature of ocean surface waves and sediment seismic noise.

The seabed acceleration and hydrodynamic pressure were recorded in FM analog mode for durations of up to 16 h, with a typical length of 8 h. For compatibility with the analog units, the digital radiotelemetry signals were converted to analog and recorded using the same FM data recorders. The signals had a frequency content in the range 0.004–0.5 Hz, controlled by bandpass filters. A digitization rate of 4 Hz was chosen to avoid signal aliasing. A 12-bit digitizer was used, giving a 72-dB dynamic range. Nonoverlapping time segments of 2048 points (8.53 min) were used in a fast Fourier transform algorithm to calculate the frequency spectra. This gives a frequency bin width of 1.953 mHz. Each time segment was demeaned and windowed using a 10% cosine taper. In this paper, we shall denote $S_{vv}(f)$ as the time-averaged vertical acceleration power spectra, $S_{pp}(f)$ as the time-averaged pressure power spectra, and $S_{vp}(f)$ as the time-averaged cross spectra between vertical acceleration and pressure. These spectra are calculated in the usual manner, being variance normalized and corrected for the frequency responses of the various instruments, amplifiers, and filters. Also, from examination of the individual time-segment variances, it was found that typical seabed pressures and accelerations were stationary for durations of 6–8 h.

These power and cross spectra are ensemble averaged over the length of the data set. From these averaged power and cross spectra, complex admittance spectra can be calculated. Seabed admittance is defined in this context as the ratio of seabed-displacement amplitude to the SG-wave amplitude at the surface. If one regards the water-wave-induced pressure as an input to a linear system, and the seabed acceleration as the output, then admittance is nothing more than a "dressed-up" transfer function. With sufficient accuracy, the water waves can be modeled using linear, small-amplitude theory. Thus the wave-induced bottom pressure P_0 is given by

$$P_0 = a\rho g/\cosh(kd), \tag{1}$$

where a is the wave amplitude at the surface (m), ρ is the water density (1025 kg/m^3), g is the gravitational acceleration (9.81 m/s^2), d is the water depth (m), and k is the water wavenumber $(2\pi/\lambda)$ given by the dispersion relation

$$\omega^2 = gk\tanh(kd), \tag{2}$$

where ω is the wave angular frequency $(2\pi f)$. Note that because of the $\cosh(kd)$ term, the wave-induced pressure falls off dramatically as kd becomes large (deeper water or higher frequency). For example, where the water depth equals the wavelength $(kd = 2\pi)$, the pressure amplitude is 0.37% of the surface value.

Then, using the definition of SG-wave-induced seabed pressure and integrating twice to get displacement, the vertical seabed admittance $\eta(f)$ is calculated from the measured transfer function between acceleration and pressure:

$$\eta(f) = [-\rho g/4\pi^2 f^2 \cosh(kd)][S_{vp}(f)/S_{pp}(f)]. \tag{3}$$

It can be shown that estimation of the transfer function using the cross spectrum as above is optimum in the presence of noise (Bendat and Piersol[36]).

Also useful to calculate is the coherence spectra for vertical admittance. Coherence is the normalized magnitude of the cross spectrum, and approaches a value of 1.0 when there is a direct cause and effect relation between the hydrodynamic pressure and the seabed response. Vertical coherence is defined:

$$\gamma_v^2(f) = |S_{vp}(f)|^2/[S_{vv}(f)S_{pp}(f)]. \tag{4}$$

Seabed admittance is used as the input data for the shear-modulus profile inversion algorithm. The coherence parameter is useful in calculating an uncertainty bound on the admittance data. As will be discussed later, the properties of SG waves limit the useful admittance data to the frequency range 0.03–0.3 Hz. Also, the uncertainty in admittance comes directly from the coherence (from Bendat and Piersol[36]):

$$\Delta\eta(f) = \eta(f)\left[(\sqrt{1-\gamma_v^2})/\gamma_v\sqrt{2N}\right], \tag{5}$$

where N is the number of time segments in the spectral averaging.

III. DISCUSSION OF RESULTS

A. Sediment motions

Surface gravity-wave-induced seabed motion can be modeled using a combination of linear water-wave theory and elastic seabed response. The sediment response has the same wavelength and phase velocity as the water wave, with the seabed displacement and water surface displacement 180° out of phase. The sediment response exhibits the same prograde particle motion as the water waves.

The seabed response is given by elastic seabed theory, derived by Yamamoto *et al.*[37,38] For a marine sediment, several simplifications are possible. Due to the low shear strength of the sediment as compared to its bulk compressibility, the sediment can be assumed incompressible. Thus the deformation is due only to shearing. Because of the low frequencies inherent to surface gravity waves (usually less than 0.3 Hz), inertial terms can be neglected. Also, because of the small shear strains (typically 10^{-6} or less) and small amplitudes of sediment motion, damping terms are quite small, and can be assumed zero if desired. These assumptions have been verified by previous BSMP measurements (Trevorrow *et al.*[15]).

Under these circumstances, it is possible to realistically predict the elastic sediment response to SG-wave-induced pressures. The vertical displacement w in a homogeneous, elastic seabed is given by Yamamoto *et al.*[37]:

$$w=(P_0/2kG)(e^{-kz}+kze^{-kz})e^{i(kx+\omega t)}, \quad (6)$$

where z is depth in the seabed (positive downwards), and G is the sediment elastic shear modulus (Pa). By substituting for the SG-wave-induced bottom pressure from Eq. (1) and evaluating Eq. (5) at the seabed surface ($z=0$), we can derive an analytic expression for vertical admittance:

$$\eta=w/a=\rho g/2kG\cosh(kd). \quad (7)$$

Note that admittance is inversely proportional to the sediment shear modulus. Thus softer sediments (such as found in the deep ocean) will exhibit larger amplitude motions. For inhomogeneous, layered seabeds, the shear modulus G is a function of depth. Thus a more complicated numerical integration of seabed displacements and stresses must be used to calculate vertical admittance (see Yamamoto,[38] Yamamoto and Torii[29]). The above approximation [Eq. (6)] is useful where the sediment properties are only approximately known, as is the case in most of the ocean. This will be used later to extrapolate observed sediment motions to deeper waters.

One of the major problems for the shear-modulus inversion is the finite bandwidth of good-quality (high-coherence) measured admittance data. This unavoidably arises from properties of the ocean-wave spectra. There is typically significant wve energy only in the frequency range 0.05–0.3 Hz. The high-frequency bound is strongly dependent on the water depth. Because the wave-induced pressure amplitude on the seabed is greatly attenuated for wavelengths comparable to or less than the water depth, we shall arbitrarily set the high-frequency limit at that frequency where the wavelength equals the water depth. For example, the cutoff frequency in 10 m of water is 0.4 Hz, while in 150 m the cutoff is 0.10 Hz. The lack of shorter wavelengths severely limits the shear-modulus inversion resolution near the seabed surface.

At the low-frequency end of the spectrum, the surface-gravity-wave energy falls away, making accurate seismic measurements difficult due to instrumental noise. A typical low-frequency seismic "falloff" from experiments conducted in 12 m of water is 0.056 Hz ($\lambda=190$ m). Since the penetration depth of the shear-modulus inversion algorithm is approximately equal to one-half of the longest wavelength of coherent admittance data, this limits the maximum penetration depth.

The other major source of ambient seismic noise in shallow continental margin sediments are "microseisms," which occur in the frequency range 0.2–10.0 Hz. The predominant propagational mode in this frequency range is a Scholte-type water–sediment interface wave. These waves are similar to Rayleigh waves, except that the presence and compressibility of a finite-depth water layer is included. Scholte waves have retrograde elliptical particle motion at the interface and decay exponentially away from the interface in both media. The phase velocity of the fundamental mode of Scholte waves is always less than that of the sediment shear waves. For water of finite depth overlaying a homogeneous sedimentary half-space, Scholte waves are weakly dispersive. The dispersion relation for the fundamental mode is given by Essen[39]:

$$\omega^4\gamma_c\tanh(\gamma_w kd)=(\rho_s/\rho_w)k^4c_s^4\gamma_w[4\gamma_c\gamma_s-(1-\gamma_s^2)^2], \quad (8)$$

where ρ_w is the water density (1025 kg/m^3), ρ_s is the bulk sediment density, k is the Scholte wavenumber ($=2\pi/\lambda$), c_w is the compressional wave speed in water (1500 m/s), c_c is the compressional wave speed in sediments, c_s is the shear-wave speed in sediments, and

$$\gamma_x=\sqrt{1-(\omega/kc_x)^2}. \quad (9)$$

For a typical sandy continental shelf sediment, it is possible to greatly simplify Eq. (8). Taking typical sediment properties as $\rho_s=2000$ kg/m^3, $c_c=2500$ m/s, and $c_s=250$ m/s, it is possible to neglect compressibility effects ($c_s\ll c_w, c_c$). This makes γ_c and γ_w approximately equal to 1.0, and we can then simplify to

$$\left(\frac{f\lambda}{c_s}\right)^4\tanh(kd)=\frac{\rho_s}{\rho_w}\left[4\sqrt{1-\left(\frac{f\lambda}{c_s}\right)^2}-\left(\frac{f\lambda}{c_s}\right)^4\right]. \quad (10)$$

This simplified expression can be easily solved for the Scholte-wave speed ($f\lambda$). For example, a 1.0-Hz Scholte wave propagating in 12 m of water on the sandy sediments specified above has a phase speed of 242 m/s. Using a six-element OBS array at the AGS site, the authors have found the seismic energy in the range 0.3–1.0 Hz to be retrograde, water/sediment interface waves (Scholte waves) traveling at $\approx$250 m/s (Goodman *et al.*[23]).

B. OBS spectra

Figure 3 shows the time-averaged vertical acceleration and hydrodynamic pressure power spectra from the George's Bank site. The pressure spectrum is due almost entirely to long "swell" waves incident from the open Atlantic Ocean, with a peak power density of 3.0×10^6 Pa^2/Hz occurring at 0.1 Hz. There are also subsidiary swell peaks at 0.075, 0.05, and 0.025 Hz (the harmonic nature of these peaks is of unknown origin). The water depth of 51 m induces a pressure "cutoff" (wavelength = water depth) at 0.18 Hz. Note, however, an indication of a wind-driven "sea" peak at 0.2 Hz. This is consistent with the measured wind speed of 7–10 m/s. Below 0.2 Hz the seismic spectrum mimics the form of the pressure spectrum. This indicates that the seabed motion is almost entirely coupled to the SG-wave-induced pressure. The peak seismic power level is 5.0×10^{-10} (m/s^2)^2/Hz at 0.1 Hz. Above 0.3 Hz, there is a strong and broad peak due to microseisms. However, there is no significant "double-frequency" pressure signal as the direct cause of these microseisms. This suggests that the microseismic waves are not being generated at this location. Notice also the quiet "notch" in the seismic spectrum in the range 0.18–0.25 Hz. As was argued in Sec. I, the true seismic background level in this notch is probably lower than 5.0×10^{-12} (m/s^2)^2/Hz.

Figure 4 shows a similar comparison to Fig. 3, only in much shallower waters (12 m) at the AGS site. Again, the vertical acceleration and pressure spectra have similar structure in the range 0.05–0.35 Hz. In this water depth, the pressure cutoff is 0.36 Hz. Note the presence of a wind-driven

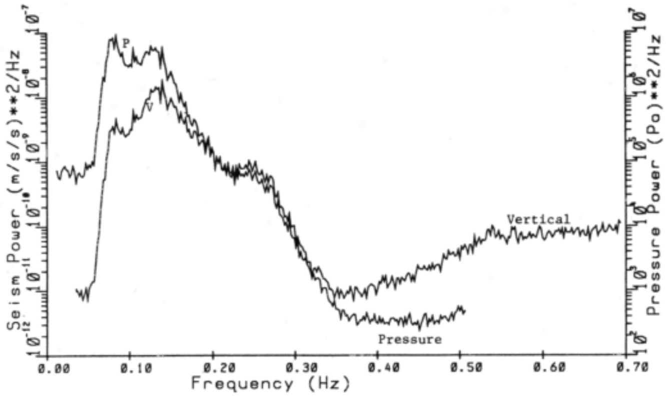

FIG. 4. Time-averaged vertical seismometer and seabed pressure power spectra from AGS site, 7 July 1988. Water depth = 12 m. Averaged over 47 time segments (6.7 h).

SG-wave peak at 0.25 Hz in both spectra. The peak seismic power level is 2.0×10^{-8} $(\mathrm{m/s^2})^2/\mathrm{Hz}$, which is some 40 times higher than shown in Fig. 3. However, the microseism power level is about an order of magnitude less than observed on George's Bank.

Figure 5 shows the time-averaged vertical admittance magnitude and coherence calculated from the data shown in Fig. 4. The coherence parameter indicates the frequency range where there is a strong seabed response to the hydrodynamic pressure. There is no coherence between pressure and seabed motion at microseismic frequencies (above 0.4 Hz). Obviously, the good-quality admittance data lies in the range 0.05–0.3 Hz. The admittance curve is a smooth function of frequency in this range. Note that admittance is a form of seabed transfer function, which depends only on the sediment properties (shear modulus) and the water depth. The wider is this high-coherence bandwidth, the better will be the shear-modulus inversion result. The width of this high-coherence frequency band is also a good indication of the quality of OBS-sediment coupling. An unburied BSMP would have a narrower high-coherence band. The vertical admittance phase (not shown) deviates by only a few degrees from 180°, supporting the assumption of nearly lossless, elastic seabed behavior.

To further demonstrate the propagational characteristics of the observed seabed motions, we can look at the cross-spectral coherence and phase between horizontally separated seismometers, as shown in Fig. 6. The two BSMP units were deployed a distance $b = 120$ m apart along a bearing $\theta_0 = 130°$. The coherence spectrum identifies two propagational bands, one for SG waves, in the range 0.05–0.15 Hz, and one for the microseisms, in the range 0.45–0.7 Hz. Following Snodgrass *et al.*,[40] the phase spectrum $\phi(f)$ can be used to extract directional information for the SG waves, since the wavelength is known from the SG dispersion relation [Eq. (2)]. Using simple geometry, the wave direction $\theta(f)$ can be calculated:

$$\theta(f) = \theta_0 \pm \alpha(f), \tag{11}$$

where

$$\alpha(f) = \arccos(\phi\lambda/360b). \tag{12}$$

The $\pm$ represents a directional ambiguity that arises from the use of only two sensors. At the AGS site, we had several other instruments deployed simultaneously. By choosing the common direction between several two-point comparisons, the directional ambiguity can be removed (also, more sophisticated directional spectrum techniques were applied). In this case, the $\theta - \alpha$ solution is appropriate. The first zero crossing in phase occurs at 0.09 Hz, which has a wavelength of 113 m and yields a wave direction of 110°. This wave direction is fairly constant across the entire SG-wave band from 0.05 to 0.15 Hz and represents swell waves incident from the open Atlantic (to the east). The fact that the measured phase and predicted λ give a constant direction of the entire

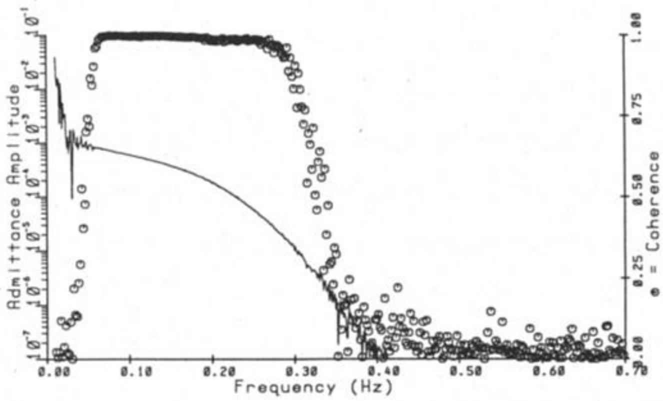

FIG. 5. Vertical admittance and coherence spectra from AGS site (data shown in Fig. 4).

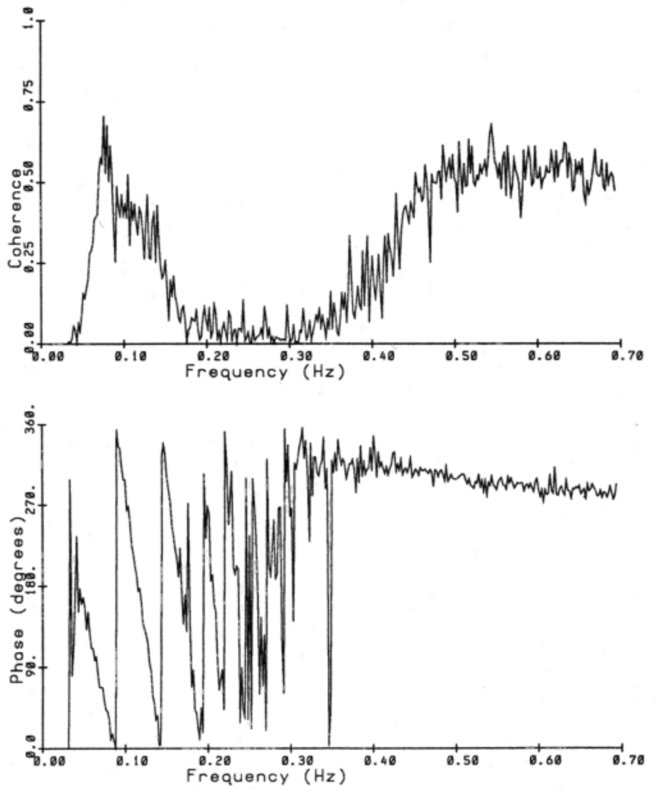

FIG. 6. Cross-spectral coherence and phase between two separated vertical seismometers at the AGS site, 7 July 1988. Units were separated by 120 m along a bearing 310°. Averaged over 54 time segments.

SG-wave band indicates that the SG-wave dispersion relation [Eq. (2)] is appropriate for these sediment motions.

In the microseism band (0.45–0.7 Hz), we do not *a priori* know the Scholte wavelength. However, the phase curve's gradual decrease from 360° is indicative of a much faster (longer wavelength) wave propagation, of the order of several hundred m/s.

Using the coherence spectrum, we can also obtain an estimate of the directional spread $\Delta\theta(f)$(deg) of the SG waves (from Snodgrass *et al.*[40]):

$$\Delta\theta(f) = (\sqrt{12/5})\,[\,(180\lambda\sqrt{1-\gamma^2})/b\pi^2\cos(\alpha)\,]. \qquad (13)$$

For the first zero crossing at 0.09 Hz, the coherence γ^2 is about 0.5, which yields a directional spread of approximately 20°.

The temporal variation of these observed seabed motions can be assessed by comparing results from two separate experiments. Figure 7 shows the vertical acceleration power spectra collected nearly a year apart at the AGS site. The differences between the two spectra may be attributed entirely to different weather conditions, as the admittance curves (1988 result shown in Fig. 5) for these two deployments were identical. In 1988, there was a higher swell energy and a wind-driven sea with peak at 0.25 Hz. In 1987, the microseism energy was about an order of magnitude higher (reason unknown).

Figure 8 shows the variation in vertical acceleration power spectra with water depth on the New Jersey shelf. Curve A comes from the AGS site (also shown in Fig. 4) in 12 m of water, curve B comes from the AMCOR 6009 site in 58 m of water, and curve C comes from the AMCOR 6010 site in 70 m of water. The pressure cutoff frequencies are 0.36, 0.16, and 0.15 Hz, respectively. Notice that the SG-wave-signal levels decrease rapidly and the peak shifts to lower frequencies in deeper waters, as expected. The microseismic power level is roughly constant at all three water depths at approximately 5.0×10^{-10} $(\mathrm{m/s}^2)^2$/Hz. Note that the microseismic power level for curve A (AGS site) is about a factor of 10 lower, but as just shown in Fig. 7, a microseismic power level similar to curves B and C was observed in 1987 at the AGS site.

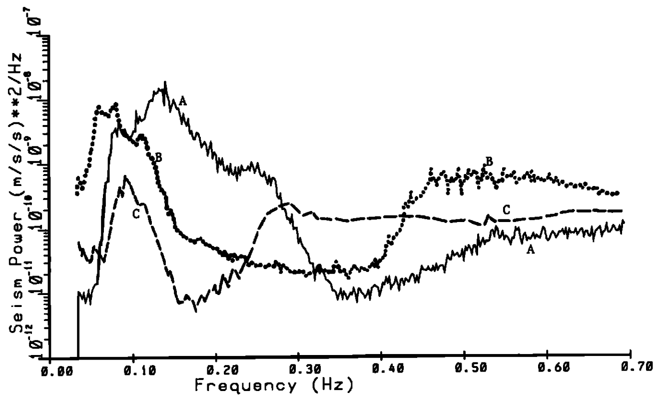

FIG. 8. Depth dependence of vertical seismometer power spectra: A = AGS site (7 July 1988), $d = 12$ m; B = AMCOR 6009 site (3 Sept. 1987), $d = 58$ m; C = AMCOR 6010 site (13 July 1988), $d = 70$ m.

C. Extrapolations to deeper water

Using the measured vertical acceleration and pressure spectra, we can calculate the SG-wave-induced seabed noise levels in deeper waters. For these calculations, we shall use the spectra measured at the AGS site (shown in Fig. 4) as representative of conditions on the shallow eastern U.S. continental shelf. We can obtain similar results using any of the measured pressure and seismic spectra. Increasing water depth influences the SG-wave-induced motions in two ways. First, deeper waters attenuate the hydrodynamic pressure on the seabed, as described by Eq. (1). A smaller pressure amplitude means smaller seabed motions. Second, the SG wavelength changes with water depth, as described by Eq. (2). At the same frequency, deeper waters cause longer wavelengths. In the following, the reference conditions (AGS site) will be denoted with the subscript 0, as in k_0 and d_0 (= 12 m), and the conditions extrapolated to a new water depth will have the subscript 1.

The SG-wave-induced bottom pressure falls off dramatically in deeper waters, as shown in Fig. 9. The pressure variation is given by

$$S_{pp1}(f) = S_{pp0}(f)\,[\cosh(k_0d_0)/\cosh(k_1d_1)\,]^2. \qquad (14)$$

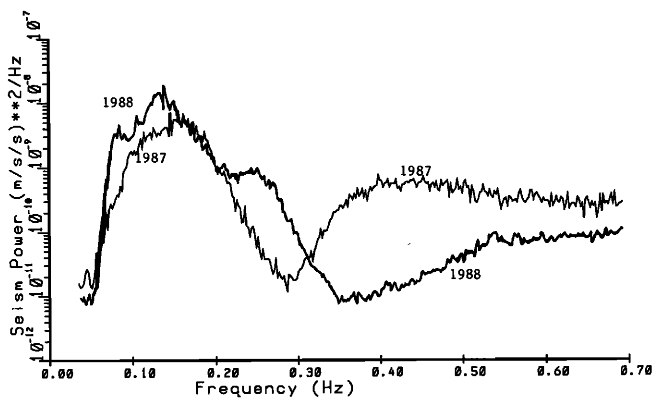

FIG. 7. Comparison of vertical seismometer power spectra from AGS site: 1987 = 29 Aug. 1987; 1988 = 7 July 1988 (46 and 47 segment averages, respectively).

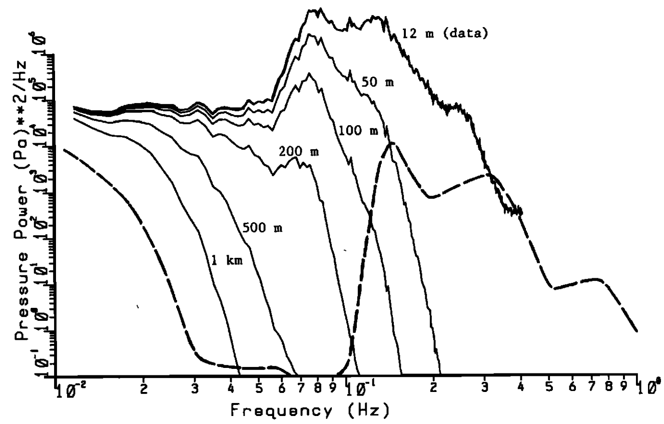

FIG. 9. Extrapolation of seabed pressure power spectrum to deeper water. Based on data from AGS site, depth = 12 m (shown in Fig. 4). Dashed line is measured pressure spectrum in 3700 m of water (from Webb and Cox[11]).

At depths of 100 m or greater, all traces of the wind-driven "sea" (0.12–0.3 Hz) are gone. The powerful open-ocean swell (0.05–0.1 Hz) peaks disappear by 1000 m. Thus in the deep ocean it should be expected that only infragravity SG waves (below 0.05 Hz) will be able to cause this single-frequency seabed motion. The dashed line shows a measured pressure power spectrum in 3700 m of water (from Webb and Cox[11]) off the coast of California. This deep-ocean measurement shows an increasing "single-frequency" pressure signal below 0.03 Hz. The large deep-ocean pressure peak (10^3–10^4 Pa^2/Hz) in the range 0.1–0.4 Hz is due to "double-frequency" SG-wave interactions. This level of DF pressure would not be observed in our shallow-water BSMP experiments because the single-frequency pressure levels are so high. However, even at frequencies above 0.4 Hz, we have not observed significant levels of wave-induced sea-bottom pressure.

Similarly, we can extrapolate the SG-wave-induced vertical acceleration to deeper water. Substituting the square root of Eq. (13) into Eq. (6), differentiating twice (multiply by $-\omega^2$), then squaring to get power, yields the variation of $S_{vv1}(f)$ with depth:

$$S_{vv1}(f) = \frac{4\pi^4 f^4}{k_1^2 G^2}\left(\frac{\cosh(k_0 d_0)}{\cosh(k_1 d_1)}\right)^2 S_{pp0}(f), \qquad (15)$$

where G is the sediment shear modulus (Pa). For the typical sandy sediments found on the continental shelf, we shall take $G = 200$ MPa. This will yield a conservative estimate of seabed acceleration power, as sandy sediments are the hardest (largest shear modulus) of commonly found seabed sediments. Silts, clays, and muds common to deeper seabeds will yield larger amplitude motions under the same SG-wave forcing. The measured pressure power spectrum at the AGS site is used as the base quantity because the measured seismic spectrum is noise dominated below 0.03 Hz.

Figure 10 predicts the seismic power spectra at various water depths given the same SG-wave conditions as measured at the AGS site. As expected, the seismic power diminishes in deeper waters. Also, we can see that the BSMP system as it presently exists would not be able to properly measure the seabed motions at water depths greater than ≈ 200 m. This is because the predicted power levels fall below the 5×10^{-12} $(m/s^2)^2$/Hz internal noise basement in the seismometer system. For comparison, the measured vertical seismic spectrum in 3660 m of water off the coast of California (from Prothero and Schaecher[9]) is shown. The broad peak at 0.25 Hz is due to microseisms. Notice that the peak microseismic power level of 3×10^{-12} $(m/s^2)^2$/Hz is similar to those measured in shallow waters (Figs. 3, 4, 7, and 8). Their spectrum does not extend to low enough frequencies to measure SG-wave-induced motion at that depth.

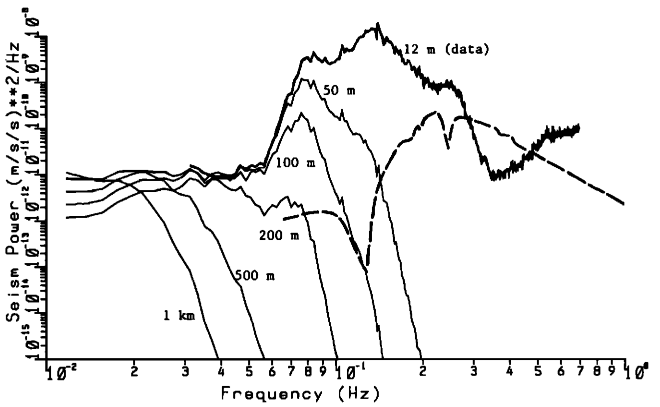

FIG. 10. Extrapolation of SG-wave-induced vertical acceleration to deeper water. Pressure and vertical acceleration data taken from AGS site, depth = 12 m (shown in Fig. 4). Seabed admittance calculated assuming sandy seabed, shear modulus = 200 MPa. Dashed line is measured vertical acceleration due to microseisms in 3660 m of water (from Prothero and Schaecher[9]).

IV. CONCLUSIONS

For shallow waters (depth < 100 m) and frequencies below 1.0 Hz, seabed seismic levels are considerably higher than in the deep ocean. Surface gravity-wave-induced seabed motion is dominant in the range 0.03–0.3 Hz. The vertical acceleration level was measured as high as 2.0×10^{-8} $(m/s^2)^2$/Hz in 12 m of water. This peak level decreases rapidly in deeper waters.

Microseisms of the Scholte type (retrograde water/sediment interface waves) were observed in the range 0.25–1.0 Hz (and probably extending to higher frequencies), with seismic levels in the range 5–10×10^{-10} $(m/s^2)^2$/Hz. This microseismic energy level was observed to be roughly constant in water depths ranging from 12–70 m. The microseismic energy level was also found to be dependent on wave and weather conditions. However, no significant levels of "double-frequency" sea-bottom pressure were observed as the cause for these Scholte waves.

A relatively quiet "notch," in the range 0.15–0.3 Hz, was observed in between the water-wave and microseismic bands. The background seismic level in this notch could not be measured because it was below the internal noise levels of the seismometer electronics. Still, it can be concluded that the seismic background level was no larger than 5.0×10^{-12} $(m/s^2)^2$/Hz.

ACKNOWLEDGMENTS

This work was supported under U.S. Office of Naval Research Contract N00014-87-G-016. The authors are grateful for this support and the continued guidance of Dr. Marshall Orr (ONR code 1125 OA). We would like to thank C. Abbott, M. Badiey, T. Nye, and K. Ando for their assistance with these experiments. We also wish to thank the Captains and crew of the R.V. ATLANTIC TWIN and R.V. CAPE HENLOPEN for their seamanship during the difficult ocean deployments.

[1] R. G. Adair, J. A. Orcutt, and T. H. Jordan, "Low-frequency Noise Observations in the Deep Ocean," J. Acoust. Soc. Am. **80**, 633–645 (1986).
[2] H. Bradner and J. G. Dodds, "Comparative Seismic Noise on the Ocean Bottom and on Land," J. Geophys. Res. **69** (20), 4339–4348 (1964).
[3] H. Bradner, J. G. Dodds, and R. Foulks, "Investigation of Microseism Sources with Ocean Bottom Seismometers," Geophysics **30** (4), 511–526 (1965).

[4]T. M. Brocher and B. T. Iwatake, "Sources of Low-frequency Ambient Seafloor Noise on a Continental Shelf," Bull. Seismol. Soc. Am. **72** (4), 1129–1142 (1982).

[5]M. A. H. Hedlin and J. A. Orcutt, "A Comparative Study of Island, Seafloor, and Subseafloor Ambient Noise Levels," Bull. Seismol. Soc. Am. **79** (1), 172–179 (1989).

[6]G. V. Latham and G. H. Sutton, "Seismic Measurements on the Ocean Floor: 1. Bermuda Area," J. Geophys. Res. **71** (10), 2545–2573 (1966).

[7]G. Latham and A. Nowroozi, "Waves, Weather, and Ocean Bottom Microseisms," J. Geophys. Res. **73** (12), 3945–3956 (1968).

[8]W. A. Prentiss and J. I. Ewing, "The Seismic Motion of the Deep Ocean Floor," Bull. Seismol. Soc. Am. **53** (4), 765–781 (1963).

[9]W. A. Prothero, Jr. and W. Schaecher, "First Noise and Teleseismic Recordings on a New Ocean Bottom Seismometer Capsule," Bull. Seismol. Soc. Am. **74** (3), 1043–1058 (1984).

[10]W. A. Schneider, P. J. Farrel, and R. E. Brannian, "Collection and Analysis of Pacific Ocean–bottom Seismic Data," Geophysics **29** (5), 745–771 (1964).

[11]S. C. Webb and C. S. Cox, "Observations and Modelling of Seafloor Microseisms," J. Geophys. Res. **91** (B7), 7343–7358 (1986).

[12]G. H. Sutton, F. Duennebier, and B. Iwatake, "Coupling of Ocean Bottom Seismometers to Soft Bottom," Mar. Geophys. Res. **5**, 35–51 (1981).

[13]G. H. Sutton and F. Duennebier, "Optimum Design of Ocean Bottom Seismometers," Mar. Geophys. Res. **9** (1), 45–65 (1988).

[14]M. Trevorrow, T. Yamamoto, A. Turgut, D. Goodman, and M. Badiey, "Very Low Frequency Ocean Bottom Seismic Noise and Coupling on the Shallow Continental Shelf," Mar. Geophys. Res. **11**(2), 129–152 (1989).

[15]M. Trevorrow, T. Yamamoto, M. Badiey, A. Turgut, and C. Conner, "Experimental Verification of Seabed Shear Modulus Profile Inversions using Surface Gravity (Water) Wave-induced Seabed Motion," Geophys. J. **93** (3), 419–436 (1988).

[16]R. A. Haubrich, W. Munk, and F. Snodgrass, "Comparative Spectra of Microseisms and Swell," Bull. Seismol. Soc. Am. **53** (1), 27–37 (1963).

[17]R. A. Haubrich and G. S. MacKenzie, "Earth Noise, 5 to 500 Millicycles Per Second: 2. Reactions of the Earth to Oceans and Atmosphere," J. Geophys. Res. **70** (6), 1429–1440 (1965).

[18]A. C. Kibblewhite and K. C. Ewans, "Wave–Wave Interactions, Microseisms, and Infrasonic Ambient Noise in the Ocean," J. Acoust. Soc. Am. **78**, 981–994 (1985).

[19]M. Longuet-Higgins, "A Theory of the Origin of Micro-seisms," Philos. Trans. R. Soc. London A **243**, 1 (1950).

[20]K. A. Hasselmann, "A Statistical Analysis of the Generation of Microseisms," Rev. Geophys. **1**, 177–210 (1963).

[21]T. T. Kadota and F. M. Labianca, "Gravity Wave-induced Pressure Fluctuations in the Deep Ocean," IEEE J. Ocean. Eng. **6** (2), 50–58 (1981).

[22]G. Latham, R. Anderson, and M. Ewing, "Pressure Variations Produced at the Ocean Bottom by Hurricanes," J. Geophys. Res. **72** (22), 5693–5704 (1967).

[23]D. Goodman, T. Yamamoto, M. Trevorrow, A. Turgut, and M. Badiey, "Directional Spectral Characteristics of Microseisms using a Shallow Water OBS Array," J. Acoust. Soc. Am. (in press) (1989).

[24]R. D. Stoll, G. M. Bryan, R. Flood, D. Chayes, and P. Manley, "Shallow Seismic Experiments using Shear Waves," J. Acoust. Soc. Am. **83**, 93–102 (1988).

[25]R. J. Urick, "Seabed Motion as a Source of the Ambient Noise Background of the Sea," J. Acoust. Soc. Am. **56**, 1010–1011 (1974).

[26]H. Schmidt and W. A. Kuperman, "Estimation of Surface Noise Source Level from Low-frequency Seismoacoustic Ambient Noise Measurements," J. Acoust. Soc. Am. **84**, 2153–2162 (1988).

[27]A. C. Kibblewhite and C. Y. Wu, "The Generation of Infrasonic Ambient Noise in the Ocean by Nonlinear Interactions of Ocean Surface Waves," J. Acoust. Soc. Am. **85**, 1935–1945 (1989).

[28]A. C. Kibblewhite and C. Y. Wu, "A Reexamination of the Role of Wave–Wave Interactions in Ocean Noise Generation," J. Acoust. Soc. Am. **85**, 1945–1957 (1989).

[29]T. Yamamoto and T. Torii, "Seabed Shear Modulus Profile Inversions using Surface Gravity (water) Wave-induced Bottom Motion," Geophys. J. R. Astron. Soc. **85**, 413–431 (1986).

[30]T. Yamamoto, M. Trevorrow, M. Badiey, and A. Turgut, "Determination of the Seabed Porosity and Shear Modulus Profiles using a Gravity Wave Inversion," Geophys. J. Int. **98**(1), 173–182 (1989).

[31]M. Trevorrow, T. Yamamoto, A. Turgut, C. Abbott, M. Badiey, D. Goodman, and K. Ando, "High Resolution Bottom Shear Modulus Profiler Experiments on the New Jersey Shelf, Summer 1987," RSMAS Tech. Rep. 88-002, University of Miami (1988).

[32]M. Trevorrow, T. Yamamoto, A. Turgut, C. Abbott, M. Badiey, D. Goodman, and K. Ando, "Summary of Seismic and Pressure Measurements Taken in July, 1988 on the New Jersey Shelf and George's Bank," RSMAS Tech. Rep. 88-005, University of Miami (1988).

[33]A. Turgut, T. Yamamoto, M. Trevorrow, M. Badiey, and C. Conner, "Bottom Shear Modulus Profiler: A Real-time Remote Sensing Instrument," submitted to ASME Transactions (1989).

[34]C. Abbott, T. Yamamoto, M. Badiey, and A. Turgut, "A Deep-water OBS Array with Real-Time Telemetry," RSMAS Tech. Rep. 87-006, University of Miami (1987).

[35]C. Cox, T. Deaton, and S. Webb, "A Deep-sea Differential Pressure Gauge," J. Atmos. Ocean Technol. **1** (3), 237–247 (1984).

[36]J. S. Bendat and A. G. Piersol, *Random Data: Analysis and Measurement Procedures* (Wiley-Interscience, New York, 1971).

[37]T. Yamamoto, H. L. Koning, H. Sellmeijer, and E. Van Hijum, "On the response of a poro-elastic bed to water waves," J. Fluid. Mech. **87**, 193–206 (1978).

[38]T. Yamamoto, "Propagator Matrix for Continuously Layered Porous Seabeds," Bull. Seismol. Soc. Am. **73**, 1599–1620 (1983).

[39]H. -H. Essen, "Model Computations for Low-velocity Surface Waves on Marine Sediments," in *Bottom Interacting Ocean Acoustics*, edited by W. Kuperman and F. Jensen, NATO Conference Series IV (1980), pp. 299–305.

[40]F. Snodgrass, G. Groves, K. Hasselmann, G. Miller, W. Munk, and W. Powers, "Propagation of Ocean Swell across the Pacific," Philos. Trans. R. Soc. London **259**, 431–497 (1966).